Effects of Spatial Hole Burning on Gain Switching in Vertical-Cavity Surface-Emitting Lasers

Joanne Y. Law and Govind P. Agrawal, *Fellow, IEEE*

***Abstract*—We present a numerical study of the effects of carrier diffusion and spatial hole-burning in vertical-cavity surface-emitting lasers under gain switching. Our model includes spatial and temporal dependences of both the optical field and the carrier density. Results show that spatial hole burning places a limit on the minimum achievable pulse width. We demonstrate that spatial hole-burning can be avoided and shorter pulses can be obtained by using an appropriate pumping geometry. We also consider the case in which the laser operates simultaneously in two transverse modes and show that transverse-mode competition induced by spatial hole burning leads to period doubling and other interesting nonlinear behavior.**

***Index Terms*—Optical pulse generation, semiconductor lasers, surface-emitting lasers, ultrafast optics.**

I. Introduction

VERTICAL-CAVITY surface-emitting lasers (VCSEL's) have been studied extensively in the past few years because of several useful characteristics such as a low threshold current, single-longitudinal-mode operation, circular output beam, and wafer-scale integrability [1], [2]. Since VCSEL's are attractive as compact light sources for applications in optical communications and interconnects, it is important to have a thorough understanding of the high-speed modulation characteristics of these devices. Indeed, dynamic characteristics of VCSEL's have been extensively studied [3]–[12], and data transmission at bit rates as high as 10 Gb/s has been demonstrated [4]. One important application of high-speed modulation is the generation of short optical pulses of picosecond durations through gain-switching [7]–[10]. Pulse widths below 20 ps with a very low timing jitter (<100 fs) have been reported [8]. The issue of pulsewidth optimization has been studied theoretically without consideration of spatial effects [10]. Since VCSEL's have relatively large transverse dimensions, spatial effects such as spatial hole burning (SHB) are expected to play an important role, especially because VCSEL's often operate in several transverse modes at high injection currents [6]. It has been shown that VCSEL's exhibit dynamic and static characteristics significantly different from those of edge-emitting lasers because of spatial effects [11], [12]. Thus, a realistic study of gain-switched operation should take into account both the temporal and spatial variations of the carrier density.

In this paper, we present the results obtained from a numerical model capable of predicting the large-signal response of VCSEL's under high-speed modulation while including all transverse effects such as carrier diffusion and SHB. This model, described in Section II, includes the spatial dependence of both the optical field and the carrier density under various modulation conditions. It is used in Section III to calculate the output pulsewidth, frequency shift, and peak power of output pulses under various modulation conditions. Section IV considers the case of a single transverse mode and shows how the pulse width can be minimized by optimizing the size of the disc-shaped contact. Section V is devoted to the study of transverse mode competition induced by SHB.

II. Computer Model and Parameters

The formalism presented below applies to an index-guided structure with a cylindrical (disc-shaped) geometry. The radius of the device corresponds to the radius of the active region, which is taken to be 10 μm. The radius of the circular region over which the laser mode is guided through a built-in index step is 4 μm. A ring or disc contact supplies current to the active region. Both the shape and dimension of the metallic contact through which the current is injected are adjustable through two parameters in our computer model. Dynamic response is studied by numerically integrating the carrier and field equations. Assuming that the VCSEL can operate in several transverse modes simultaneously, the electric field is expressed as

$$\mathbf{E}(r,\phi,z,t)=\frac{1}{2}\sum_{i=1}^{n}\hat{\mathbf{e}}_i E_i(t)\psi_i(r,\phi)\exp[i(\beta_i z-\omega_i t)] \quad (1)$$

where n is the total number of transverse modes under consideration, $\psi_i(r,\phi)$ is the spatial distribution of the ith mode, and $E_i(t)$, β_i, and ω_i are the amplitude, the propagation constant, and the frequency of that mode. The polarization unit vector $\hat{\mathbf{e}}_i$ is allowed to be different for different modes.

By substituting (1) into the Maxwell equations, the wave equation can be separated into spatial and temporal parts for each mode. The spatial part of the mode is obtained by solving the eigenvalue equation

$$\nabla_T^2\psi_i(r,\phi)+\left\{\epsilon(r,\phi)\frac{\omega_i^2}{c^2}-\beta_i^2\right\}\psi_i(r,\phi)=0 \quad (2)$$

Manuscript received August 26, 1996; revised November 11, 1996. This work was supported in part by the U.S. Army Research Office and by the National Science Foundation under Grant PHY94-15583.

The authors are with the Institute of Optics and Rochester Theory Center, University of Rochester, Rochester, NY 14627 USA.

Publisher Item Identifier S 0018-9197(97)01571-6.

where ∇_T^2 is the transverse Laplacian, and $\epsilon(r,\phi)$ is the dielectric constant of the VCSEL structure considered; $\epsilon(r,\phi)$ is assumed to be constant in the z direction. If $\epsilon(r,\phi)$ is also ϕ independent, the solutions of $\psi_i(r,\phi)$ of (2) correspond to the linearly polarized LP_{mn} modes, which are well known in the context of optical fibers [13]. Consistent with the index-guided nature of the structure, the spatial distribution of each guided mode, $\psi_i(r,\phi)$, is assumed to be independent of time. Since carrier-induced changes in the refractive index are typically two orders of magnitude smaller than the built-in refractive index difference (about 0.1) responsible for index guiding, waveguiding properties of an index-guided VCSEL are not significantly affected by temporal changes in the carrier density. This assumption greatly reduces the amount of computation required, but spatial effects are still taken into account through gain saturation.

The evolution of mode amplitude $E_i(t)$ is governed by [15]

$$\frac{dE_i}{dt} = \frac{1}{2}\{(1-i\alpha)G_i(t) - \gamma_i\}E_i \tag{3}$$

where α is the linewidth enhancement factor, and $G_i(t)$ and γ_i are the gain and cavity loss for the ith mode.

The carrier density, $N(r,\phi,t)$, is obtained by solving [11]

$$\frac{\partial N}{\partial t} = D\nabla_T^2 N + \frac{J(r,\phi)}{qd} - \frac{N}{\tau_e} - BN^2 - \frac{1}{d}\sum_{i=1}^{n} G_{\mathrm{local}}(r,\phi,t)|E_i(t)|^2|\psi_i(r,\phi)|^2. \tag{4}$$

The first term on the right side corresponds to carrier diffusion, the second term to current injection, the third term to nonradiative carrier recombination, the fourth term to spontaneous recombination, and the last term to stimulated emission. τ_e is the carrier lifetime due to nonradiative recombination, D is the diffusion coefficient, B is the spontaneous recombination coefficient, and $J(r,\phi)$ is the injection current density. Equation (4) is written in cylindrical coordinates with ∇_T^2 representing the transverse Laplacian. The effects of spontaneous emission can be included by adding a Langevin-noise source term [15] to the right side of (3). Its inclusion is essential for studying noise-related effects such as pulse-to-pulse jitter. Since we are interested only in the average characteristics of gain-switched pulses, we ignore spontaneous emission in this study.

The local gain G_{local} is assumed to be linearly proportional to the carrier density. The gain for each mode in (3) is given by the spatial average of local gains weighed by the spatial distribution of that mode:

$$G_i(t) = \frac{\langle G_{\mathrm{local}}(r,\phi,t)|\psi_i(r,\phi)|^2\cos^2(\beta_i z)\rangle}{\langle|\psi_i(r,\phi)|^2\cos^2(\beta_i z)\rangle} \tag{5}$$

where the angle brackets denote average over the active volume, and

$$G_{\mathrm{local}}(r,\phi,t) = a_0 v_g\{N - N_T\}\{1 - \epsilon_{\mathrm{NL}}|E_i(t)|^2\}. \tag{6}$$

Here, $N(r,\phi,t)$ is the local carrier density, a_0 is the gain cross section, N_T is the carrier density at transparency, v_g is the group velocity, and ϵ_{NL} is the nonlinear-gain parameter.

TABLE I
DEVICE PARAMETERS USED IN SIMULATIONS

Cavity length L_{eff}	2 μm
Active-region thickness (3 QWs)	3×8 nm
Radius of device	10 μm
Radius of index-guiding region	4 μm
Diffusion constant D	30 $\mathrm{cm^2 s^{-1}}$
Nonradiative recombination time τ_e	5 ns
Bimolecular recombination coefficient B	1×10^{-10} $\mathrm{cm^3 s^{-1}}$
Refractive indices n_1, n_2	3.4, 3.5
Wavelength λ	0.875 μm
Gain cross-section a_0	2.0×10^{-16} $\mathrm{cm^2}$
Carrier density at transparency N_T	2.2×10^{18} $\mathrm{cm^{-3}}$
Linewidth enhancement factor α	3.0
Mirror reflectivities R_1, R_2	0.995
Internal loss α_{int}	20 $\mathrm{cm^{-1}}$
Longitudinal confinement factor Γ_l	0.012
Nonlinear-gain parameter ϵ_{NL}	0.05×10^{-17} $\mathrm{cm^3}$
Modulation frequency f_m	2–4 GHz
Bias level J_b/J_{th}	0.95

For gain-switching, the injected current density in (4) is taken to be of the form

$$J(r,t) = \begin{cases} J_b + J_m \sin(2\pi f_m t) & \text{if } r_o < r < r_a \\ 0 & \text{otherwise} \end{cases} \tag{7}$$

where J_b is the bias current density, J_m is the modulation current density, f_m is the modulation frequency, and r_o and r_a are the radii of the ring contact over which the current is injected. For a disc contact, $r_o = 0$ and r_a varies in the range 0.5–4 μm. Relevant device parameters used for numerical simulations are displayed in Table I.

Two approximations made above require justification. First, it has been shown that for a quantum-well active region, the gain is better approximated by a logarithmic than a linear function of the carrier density [16]. We adopt the linear-gain approximation since its use makes possible the implementation of a fast numerical algorithm based on the tridiagonalization of a matrix representing the carrier equation (discussed below). To justify its use, the current bias for the laser is chosen close to the threshold so that the total carrier density is expected to remain nearly constant. Second, by setting the injection current to zero outside the contact area, our model neglects current spreading effects. Such effects must be included for a realistic comparison of the numerical results with the experiments. However, the results presented here are not expected to change qualitatively when current spreading is included.

The carrier and field equations [(3) and (4)] are integrated numerically using a finite-difference method in both the temporal and spatial domains. The temporal domain is discretized into uniform steps each of 0.1 ps. To ensure that the transients have died out, gain-switched pulse characteristics are obtained after integrating the rate equations over a temporal window of 8 ns, which is much larger than the damping time of relaxation oscillations. The initial conditions can be chosen quite arbitrarily (within reason). In our simulations, for fast convergence to the steady-state pulse-train solution, the initial values of the field and carrier density correspond to the CW

operation of the laser when pumped two times above threshold. The carrier equation requires an implicit solution in the radial direction due to coupling introduced by the diffusion term. To solve for $N(r)$ at any given point in time, the spatial domain is divided evenly into $M = 100$ steps. Our radial mesh runs from δr to $R = M\delta r$, where $\delta r = 0.1$ μm is the spatial resolution, and $R = 10$ μm is the radius of the device. The point $r = 0$ is excluded because of the singularity associated with the Laplacian term. The boundary conditions $N(0) = N(\delta r)$ and $N(R) = 0$ are used. Since the diffusion term involves a second-order derivative of $N(r)$, each $N(r)$ is coupled only to its nearest neighbors $N(r+\delta r)$ and $N(r-\delta r)$. Therefore, provided that the gain is a linear function of $N(r)$, the carrier equation can be put into a tridiagonal matrix form, which can be easily inverted to obtain a solution for $N(r)$. In spite of the matrix inversion involved, the computer code is reasonably fast. A typical run takes less than 5 min on a Sparc 5 workstation.

III. Effect of Modulation Current and Frequency

We study the effects of modulation frequency and modulation current on characteristics of gain-switched pulses by using the following procedure. First, the threshold current density $J_{\rm th}$ is found by simulating CW operation for a total duration of 5 ns at various current levels. The current is increased through steps of 0.1 mA and simulations are repeated until the output power first exceeds 1 μW, which is defined as the threshold condition. Since spontaneous noise has not been included in our study, the definition of threshold power is somewhat arbitrary. Obviously, the threshold current depends on the contact geometry as well as the diffusion constant.

Output pulse trains were obtained by setting $J_b/J_{\rm th} = 0.95$ and $f_m = 2.5$ GHz in (7) for several values of modulation indexes $J_m/J_{\rm th}$. We consider the range of values of the modulation index $J_m/J_{\rm th}$ for which the device produces stable, regular gain-switched pulses at the modulation frequency. For small values of the modulation index, the device cannot respond fast enough, and the output power oscillates at a subharmonic of the modulation frequency [17]. By contrast, for large values of the modulation index, multiple relaxation-oscillation peaks are excited by a single current pulse. An estimate of the maximum modulation frequency at a given modulation current is provided by the relaxation-oscillation frequency. For an effective carrier lifetime of 3 ns and photon lifetime of 2.5 ps, the relaxation-oscillation frequency is calculated to be 2.5 GHz near three times above threshold under CW operation. For $J_b/J_{\rm th} = 0.95$, an time-averaged current of three times above threshold corresponds to a modulation index of $J_m/J_{\rm th} = 5$. Indeed, numerical simulations show that the range of values $7 \leq J_m/J_{\rm th} \leq 11$ correspond to stable operation at the modulation frequency.

The shapes and widths of gain-switched pulses are shown in Fig. 1(a) for modulation indexes $J_m/J_{\rm th} = 8$–11 at a modulation frequency of $f_m = 2.5$ GHz and a bias of $J_b/J_{\rm th} = 0.95$. The current pulse shape is also shown for comparison by a dashed line. The bias level $J_b/J_{\rm th}$ is fixed at 0.95 in all cases, since it has been observed experimentally

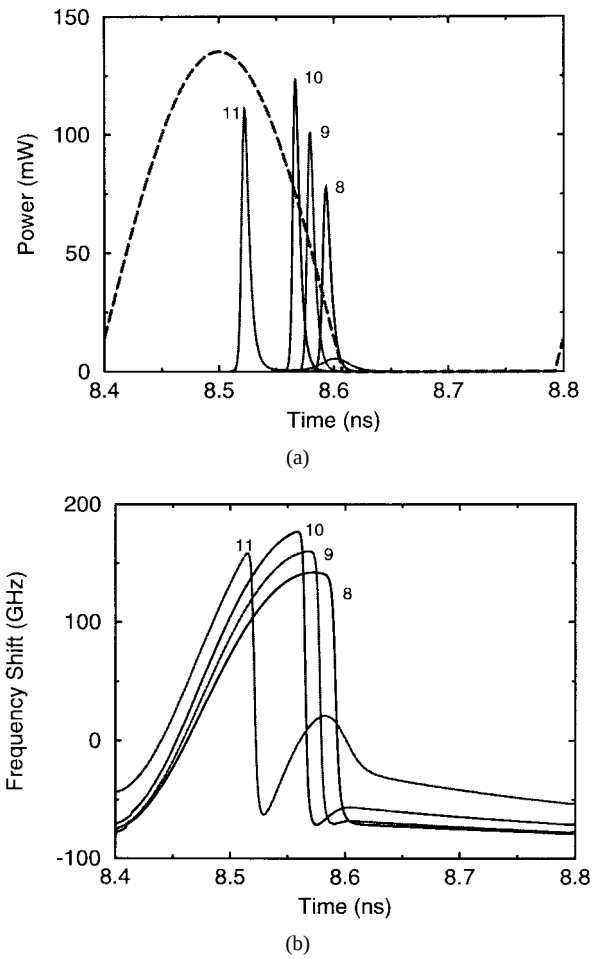

Fig. 1. (a) Pulse shapes and (b) frequency-shift profiles of gain-switched pulses obtained through 2.5-GHz sinusoidal modulation of a VCSEL biased at $J_b/J_{\rm th} = 0.95$. Dashed line shows the current pulse for comparison. The values of $J_m/J_{\rm th}$ are indicated next to each trace. Other parameter values are given in Table I.

that the optimum bias point occurs slightly below threshold [14]. As $J_m/J_{\rm th}$ increases, carrier density builds up faster. As a result, the output pulse shortens, and the delay between the current pulse and the output pulse decreases. Eventually, the delay becomes so short that a second relaxation-oscillation peak appears, as seen in Fig. 1(a) for $J_m/J_{\rm th} = 11$. There exists an optimum value of $J_m/J_{\rm th}$ at which the pulse width is minimum. For the parameters used in Fig. 1(a), the minimum pulse width of about 6 ps occurs for $J_m/J_{\rm th} \approx 10$.

Fig. 1(b) shows the frequency shift $\Delta\nu = -(1/2\pi)(d\phi/dt)$ as a function of time corresponding to the pulse shapes of Fig. 1(a), where ϕ is the optical phase. This frequency shift results from α-induced index changes which follow gain variations. Therefore, as the pulse width decreases and the peak power increases at higher values of J_m, the frequency shift is expected to increase, since high peak powers and small pulse widths are associated with a higher rate of change of photon density. The most noteworthy feature of Fig. 1(b) is a large and sudden change ($\sim$230 GHz) in the carrier frequency occurring near the pulse peak. The magnitude of the jump increases with the modulation index. It is this feature that broadens the pulse spectrum considerably compared with that

TABLE II
OUTPUT PULSE CHARACTERISTICS AT DIFFERENT MODULATION FREQUENCIES

Modulation frequency f_m (GHz)	2	3	4
Optimal value of J_m/J_{th}	8.0	12.4	17.8
Minimum pulse width (ps)	7.0	6.3	5.7
Peak power (mW)	111	138	173
Maximum frequency shift (GHz)	232	270	288

of a transform-limited pulse (about 70 GHz for a pulse with duration of 6 ps).

Output pulse characteristics for $f_m = 2$–4 GHz are shown in Table II. The optimal modulation index $J_m/J_{\rm th}$ is observed to increase with modulation frequency, as shown in Table II. This behavior can be understood by noting that the bandwidth of a VCSEL is limited by the relaxation-oscillation frequency, which increases with an increase in average input power. Therefore, higher modulation currents are required at higher modulation frequencies. It is also found that as the modulation frequency increases, the minimum pulse width decreases, and therefore the maximum frequency shift also increases. The maximum frequency shift is defined as the difference between the maximum and minimum shifts.

For the rest of this paper, we fix the modulation frequency at 2.5 GHz since this value is consistent with the OC-48 level of the SONET and STS-16 level of the SDH. We examine the effects of carrier diffusion, pumping geometry, and multiple-transverse-mode operation. SHB is included in all numerical simulations since it is found to affect the gain-switching dynamics considerably.

IV. SINGLE-MODE OPERATION

We first consider the case in which the VCSEL operates in a single transverse mode throughout the gain-switching process. In practice, this behavior can be realized by using a disc contact of 2–3-μm radius such that current is injected only over a small central part of the VCSEL top area. The $\rm LP_{01}$ mode is then preferentially excited.

A. Disc Contact

The effect of carrier diffusion is studied by comparing the results obtained by using diffusion constants of 30 $\rm cm^2{\cdot}s^{-1}$ and 1 $\rm cm^2{\cdot}s^{-1}$, respectively. A disc contact of 2-μm radius is used. The injected current follows (7) with $r_o = 0$, $r_a = 2$ μm, $J_b/J_{\rm th} = 0.95$ and $f_m = 2.5$ GHz. The changes in the pulsewidth and the frequency shift with modulation index $J_m/J_{\rm th}$ are plotted in Fig. 2. Results are shown for the range of modulation indexes which corresponds to the regime of stable, regular output pulse trains (one pulse per modulation cycle), as discussed in the previous section. It is found that the main effect of diffusion is to shift the optimal modulation index to lower values. In fact, for a given value of $J_m/J_{\rm th}$, shorter pulses are obtained when carrier diffusion is taken into account. In short, diffusion facilitates pulsing operation.

To understand the physical origin of this somewhat surprising result, the carrier-density profiles at the peaks of the gain-switched pulses are plotted in Fig. 3 for $D = 1$ (dashed) and 30 $\rm cm^2{\cdot}s^{-1}$ (solid). No spatial hole is observed for $D =$ 30 $\rm cm^2{\cdot}s^{-1}$, whereas a deep spatial hole appears when carrier diffusion is negligible ($D = 1$ $\rm cm^2{\cdot}s^{-1}$). This feature suggests that the well-known phenomenon of SHB affects the gain-switching dynamics. The deep spatial hole for the case of $D = 1$ $\rm cm^2{\cdot}s^{-1}$ reduces the overlap between the fundamental $\rm LP_{01}$ mode and the carrier profile. Consequently, the mode sees effectively less gain at a given modulation index for $D =$ 1 than for $D = 30$ $\rm cm^2{\cdot}s^{-1}$. This feature explains the shift to higher modulation indexes in the former relative to the latter case. It also illustrates that spatial and temporal effects are coupled in VCSEL's through gain saturation, and this spatio-temporal coupling plays an important role in VCSEL dynamics.

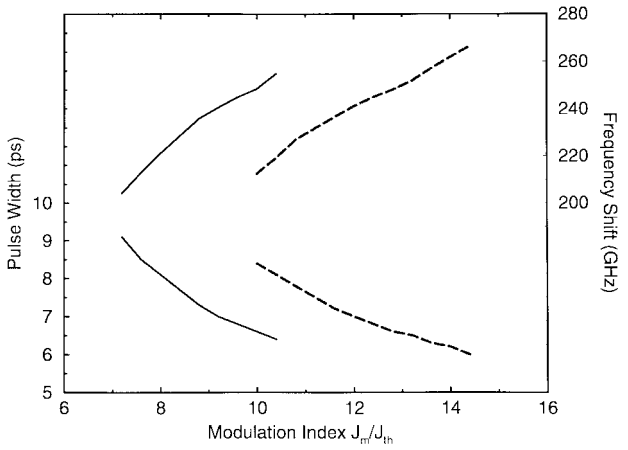

Fig. 2. Variations of pulse width (bottom traces) and frequency shift (top traces) with modulation index $J_m/J_{\rm th}$ for $D = 30$ $\rm cm^2{\cdot}s^{-1}$ (solid) and $D = 1$ $\rm cm^2{\cdot}s^{-1}$ (dashed). The modulation frequency is 2.5 GHz.

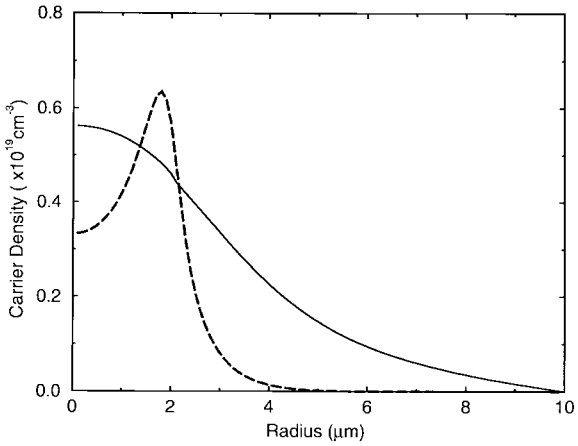

Fig. 3. Radial carrier-density profiles for $D = 30$ $\rm cm^2{\cdot}s^{-1}$ (solid) and $D =$ 1 $\rm cm^2{\cdot}s^{-1}$ (dashed) at the peak of gain-switched pulses. The value of $J_m/J_{\rm th}$ is 10.

Because of the importance of carrier diffusion, the size of the disc contact is likely to be important. Devices with disc-contact radii ranging from 0.5 to 3.5 μm were simulated to answer this question. In all cases, the modulation index is optimized to produce the shortest pulse. The minimum attainable pulsewidth and the corresponding frequency shift are plotted in Fig. 4 as a function of the disc-contact radius. A shallow minimum occurs for contact radius in the range

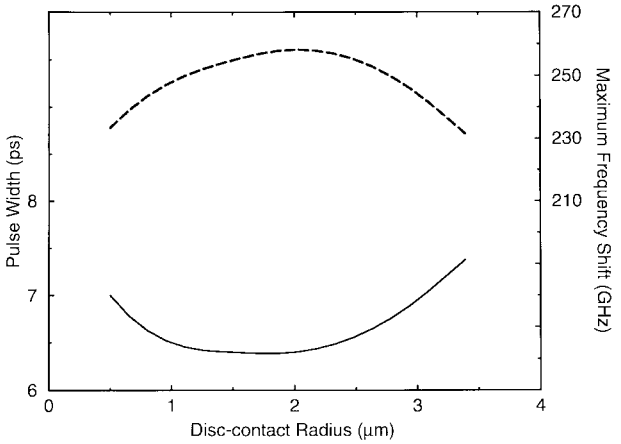

Fig. 4. Variation of pulsewidth (solid) and frequency shift (dashed) with disc-contact radius. In all cases, the modulation current is optimized to produce the shortest pulse.

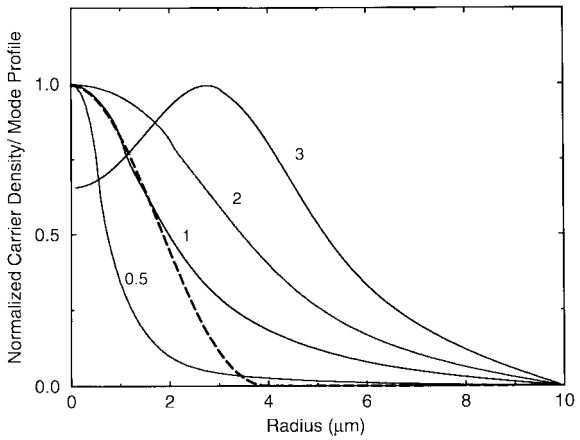

Fig. 5. Radial carrier-density profiles at the peak of thegain-switched pulse for several disc-contact radii (shown in μm) The dashed line corresponds to the spatialdistribution of the LP_{01} mode. The modulation parameters are $f_m = 2.5$ GHz, $J_b/J_{\mathrm{th}} = 0.95$, and $J_m/J_{\mathrm{th}} = 10$.

1–2 μm. The optimum range of the contact radius is likely to depend on the size of the index-guiding region, which controls the mode diameter.

To understand the origin of the pulsewidth minimum seen in Fig. 4, the carrier-density profiles at the peak of the gain-switched pulse are calculated and plotted in Fig. 5 for contact radii 0.5–3.5 μm. The results show that the size of the spatial hole burnt in the carrier-density distribution through gain saturation can be controlled by the size of the disc contact. Indeed, there is *no* spatial hole for contact radii 1–2 μm, the range that corresponds to the regime of minimum pulse widths in Fig. 4. The spatial distribution of the LP_{01} mode is illustrated by the dashed line in Fig. 5. Clearly, the spatial overlap between the mode and the carrier-density profiles is maximized for a contact radius of about 1 μm. Consequently, carriers are utilized most efficiently, and gain-switching produces the shortest pulse. Although there is no spatial hole for $r_a < 1$ μm, the pulsewidth increases because of a reduction in overlap.

To conclude, the above results suggest that by reducing the disc-contact area, the effect of SHB is reduced. Further, by maximizing the overlap between the mode and carrier-density profiles, the shortest possible pulses are obtained from VCSEL's.

TABLE III
COMPARISON OF OUTPUT PULSE CHARACTERISTICS FOR THE MODES LP_{01} AND LP_{11} UNDER SINGLE-MODE OPERATION

Parameter	LP_{01}	LP_{11}
Pumping geometry	0-2 μm disc	2-4 μm ring
Optimal value of J_m/J_{th}	10.4	8.2
Minimum pulse width (ps)	6.4	9.3
Peak power (mW)	132	104
Maximum frequency shift (GHz)	254	181

B. Ring Contact

A ring contact is often used in practice to facilitate the emission of laser output from the top mirror. However, its use excites higher order modes which saturate the gain differently, resulting in a different spatial profile for the carrier density. This section discusses how gain-switching dynamics is affected by the use of a ring contact.

A ring contact of an inner radius of 2 μm and an outer radius of 4 μm is used in numerical calculations. Such a contact preferentially excites the first-order transverse mode. The modulation index is optimized to give the shortest pulse in both cases. Table III compares the pulse characteristics such as the minimum width, the corresponding peak power, and frequency shift for the two cases of disc and ring contacts, which correspond to the excitation of LP_{01} and LP_{11} modes, respectively. The main feature is that the minimum pulse width is larger by about 50% when the LP_{11} mode is the dominant VCSEL mode.

The two transverse modes show significantly different gain-switched output characteristics. This is due to a combination of spatial effects introduced through different pumping geometries (contact areas) and different spatial distributions of the two modes. To understand the difference, the carrier-density and mode-intensity profiles are plotted in Fig. 6 for each of the two cases. The optimal modulation index is used in each case. Clearly, the LP_{01} mode has a much better overlap with the carrier-density profile than the LP_{11} mode. This results in gain-switched pulses with a much shorter pulsewidth.

V. MULTI-MODE OPERATION

Since VCSEL's can operate in several transverse modes simultaneously when a wide disc-shaped contact is used, it is interesting to study how the dynamics of gain-switching is affected by mode competition induced by SHB. We investigate gain-switching under the two-mode operation at a modulation frequency of 2.5 GHz. The pump current is supplied through a disc contact of radius 4 μm, which is equal to the radius of the index-step region. The two transverse modes excited are LP_{01} and LP_{11}. Results using a disc contact of radius 2 μm will also be presented for comparison.

Consider first the case of 2-μm-radius disc contact so that the VCSEL operates in a single transverse mode LP_{01}. Fig. 7 shows the gain-switched pulse trains obtained for $J_m/J_{\mathrm{th}} =$ 10, 12, and 15. A regular periodic pulse train is observed

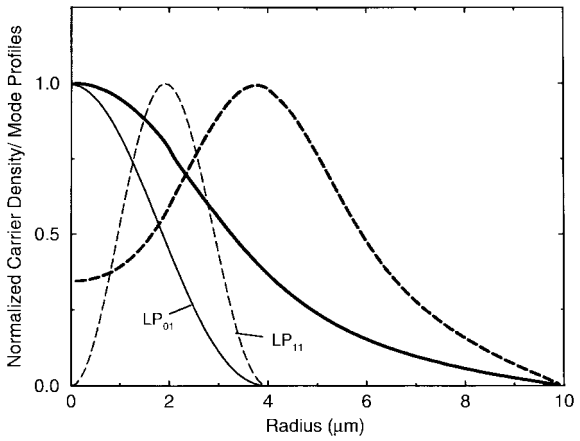

Fig. 6. Radial carrier-density profiles (bold lines) and spatial intensity distributions (lighter lines) of the modes. The solid lines correspond to the case of a 2-μm radius disc contact, and the dashed lines correspond to that of a 2-μm ring contact with inner and outer radii of 2 and 4 μm. The optimal value of modulation index is used in each case.

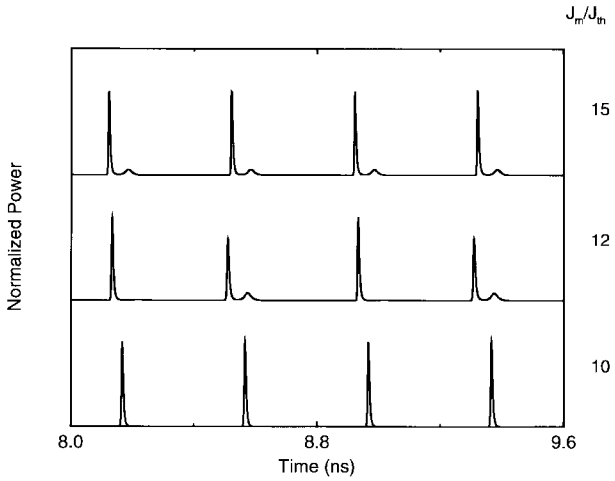

Fig. 7. Gain-switched pulse trains when the VCSEL operates in the fundamental LP_{01} mode. The values of J_m/J_{th} are indicated on the right margin. A disc contact of radius 2 μm is used. Other modulation parameters are $f_m = 2.5$ GHz and $J_b/J_{\mathrm{th}} = 0.95$.

for J_m/J_{th} of up to 10, beyond which a transition to period doubling occurs. The trace for $J_m/J_{\mathrm{th}} = 12$ shows this transition clearly. Interestingly enough, the period-one state is restored for $J_m/J_{\mathrm{th}} \geq 14$ although the pulses have a two-peak structure. No transition to chaos is observed.

The dynamical behavior becomes much more interesting when a 4-μm-wide disc contact is used so that the VCSEL operates in the LP_{01} and LP_{11} transverse modes simultaneously. Fig. 8 shows the gain-switched pulse trains under identical conditions of Fig. 7 except for a wider 4-μm contact. Solid and dotted traces correspond to the LP_{01} and LP_{11} modes, respectively. At different values of J_m/J_{th}, various kinds of nonlinear behaviors are possible, such as period-two oscillations ($J_m/J_{\mathrm{th}} = 15$), and "chaotic" behavior ($J_m/J_{\mathrm{th}} = 10$ and 12). Although regimes of chaos are found, no clear route to chaos could be identified. However, the two modes exhibit mode competition at all values of modulation currents. The LP_{11} mode peaks only when the

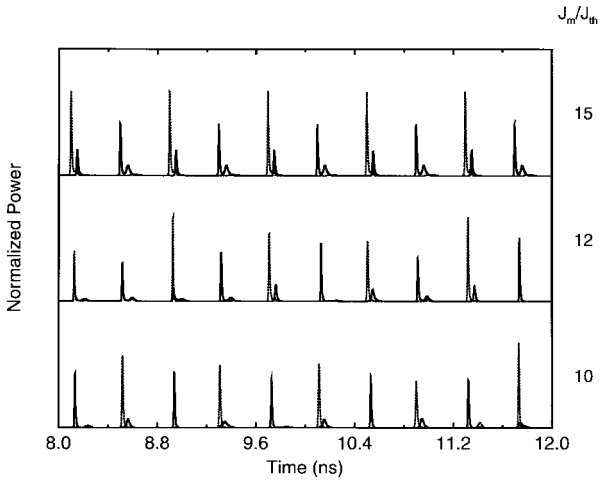

Fig. 8. Gain-switched pulse trains under operating conditions identical to those of Fig. 7 except for a 4-μm disc contact so that the VCSEL operates in two transverse modes simultaneously. The solid and dotted lines correspond to the LP_{01} and LP_{11} modes, respectively.

LP_{01} mode has little power, which is an evidence of strong mode competition. This behavior is sometimes referred to as the antiphase dynamics. Significant SHB in the region where the two transverse modes overlap leads to strong mode competition. Indeed, transverse mode competition has been observed experimentally under pulsed operation [7], and chaos has been observed experimentally in VCSEL's operating in two transverse modes under dc excitation [18]. We have also studied the impact of nonlinear gain on gain switching by varying ϵ_{NL} in the range 0–2 $\times$ 10^{-17} cm^3. Although the single-mode results shown in Figs. 1–6 remain qualitatively the same, the pulse trains shown in Figs. 7 and 8 change considerably with ϵ_{NL}. In particular, the period-doubling behavior disappears when ϵ_{NL} exceeds a critical value of $\sim$ 0.1 $\times$ 10^{-17} cm^3 [19].

VI. Conclusion

We have studied spatial effects in gain-switched VCSEL's using a computer model which incorporates spatial dependences of both the optical field and the carrier density. The effects investigated include modulation current, modulation frequency, carrier diffusion, pumping geometry, and multimode operation.

It is found that output pulse characteristics depend critically on modulation conditions. In particular, there exists an optimal modulation index J_m/J_{th} where the pulse width is minimum. Typical pulse widths are about 6 ps for the device parameters shown in Table I. The optimal modulation condition is found to be affected by the modulation frequency and pumping geometry.

The disc-contact area is shown to have a significant effect on gain-switching characteristics. Spatial holes in the carrier profile are responsible for the deterioration of device performance. With a disc-contact radius of smaller than 2 μm, spatial holes are eliminated. However, we find that the shortest pulses are obtained for disc-contact radii of 1–2 μm, the range that corresponds to maximum overlap between the spatial

distributions of the lasing mode and the carrier density. It is also found that the process of diffusion effectively increases the optimal modulation index. Since diffusion smoothes out spatial inhomogeneities in the carrier profile, it improves the spatial overlap between the mode and carrier-density profiles at a given modulation index, which results in more efficient utilization of carriers.

Pumping geometry also plays a critical role. It is shown that a ring contact excites a higher order transverse mode, which produces different gain-switched characteristics simply because the spatial overlap between the mode and carrier density profile is altered. For the case of a disc contact of 4 μm, two-mode operation results. Anticorrelated periodic oscillations are observed for all values of J_m/J_{th} investigated. Mode competition induced through SHB leads to quite interesting nonlinear dynamics. This behavior is a consequence of spatio-temporal coupling.

REFERENCES

[1] T. E. Sale, *Vertical-Cavity Surface-Emitting Lasers*. New York: Wiley, 1995.

[2] C. J. Chang-Hasnain, in *Semiconductor Lasers: Past, Present and Future*, G. P. Agrawal, Ed. Woodbury, NY: AIP Press, 1995, ch. 5.

[3] S. F. Yu, "Dynamic behavior of vertical-cavity surface-emitting lasers," *IEEE J. Quantum Electron.*, vol. 32, pp. 1168–1179, 1996.

[4] U. Fiedler, G. Reiner, P. Schnitzer, and K. J. Ebeling, "Top surface-emitting vertical-cavity laser diodes for 10-Gb/s data transmission," *IEEE Photon. Technol. Lett.*, vol. 8, pp. 746–748, 1996.

[5] O. Buccafusca, J. L. A. Chilla, J. J. Rocca, C. Wilmsen and S. Feld, "Ultrahigh frequency oscillations and multimode dynamics in vertical cavity surface emitting lasers," *Appl. Phys. Lett.*, vol. 67, pp. 185–187, 1995.

[6] C. J. Chang-Hasnain, J. P. Harbison, G. Hasnain, A. C. Von Lehmen, L. T. Florez, and N. G. Stoffel, "Dynamic, polarization and transverse mode characteristics of VCSEL's," *IEEE J. Quantum Electron.*, vol. 27, pp. 1402–1408, 1991.

[7] O. Buccafusca, J. L. A. Chilla, J. J. Rocca, S. Feld, and C. Wilmsen, "Transverse mode dynamics in vertical cavity surface emitting lasers excited by fast electrical pulses," *Appl. Phys. Lett.*, vol. 68, pp. 590–592, 1996.

[8] P. Pepelijugoski, J. Lin, J. Gamelin, M. Hong, and K. Y. Lau, "Ultralow timing jitter in electrically gain-switched vertical cavity surface emitting lasers," *Appl. Phys. Lett.*, vol. 62, pp. 1588–1590, 1993.

[9] J. M. Wiesenfeld, G. Hasnain, J. S. Perino, J. D. Wynn, R. E. Leibenguth, and Y. H. Wang, "Gain-switched GaAs vertical-cavity surface-emitting lasers," *IEEE J. Quantum Electron.*, vol. 29, pp. 1996–2005, 1993.

[10] L. G. Melcer, J. R. Karin, R. Nagarajan, and J. E. Bowers, "Picosecond dynamics of optical gain switching in vertical-cavity surface emitting lasers," *IEEE J. Quantum Electron.*, vol. 27, pp. 1417–1425, 1991.

[11] A. Valle, J. Sarma, and K. Shore, "Dynamics of transverse mode competition in VCSEL diodes," *Opt. Commun.*, vol. 115, pp. 297–302, 1995.

[12] A. Valle, J. Sarma, and K. A. Shore, "Spatial holeburning effects on the dynamics of vertical-cavity surface-emitting laser diodes," *IEEE J. Quantum Electron.*, vol. 31, pp. 1423–1431, 1995.

[13] D. Marcuse, *Theory of Dielectric Optical Waveguides.* New York: Academic, 1991, p. 73.

[14] K. Y. Lau, "Gain switching of semiconductor injection lasers," *Appl. Phys. Lett.*, vol. 52, pp. 257–259, 1988.

[15] G. P. Agrawal and N. K. Dutta, *Semiconductor Lasers*, 2nd ed. New York: Van Nostrand Reinhold, 1993, ch. 6.

[16] T. Makino, "Analytical formulas for the optical gain of quantum wells," *IEEE J. Quantum Electron.*, vol. 32, pp. 493–501 1995.

[17] W. F. Ngai and H. F. Liu, "'Observation of period doubling, and period quadrupling in a directly modulated 1.55 μm InGaP distributed feedback laser diode," *Appl. Phys. Lett.*, vol. 62, pp. 2611–2613, 1993.

[18] D. A. Richie, T. Zhang, K. D. Choquette, R. E. Lebenguth, J. C. Zachman, and N. Tabatabaie, "Chaotic dynamics of mode competition in a vertical-cavity surface-emitting laser diode under dc excitation," *IEEE J. Quantum Electron.*, vol. 30, pp. 2500–2506, 1994.

[19] G. P. Agrawal, "Effect of gain nonlinearities on period doubling and chaos in directly modulated semiconductor lasers," *Appl. Phys. Lett.*, vol. 49, pp. 1013–1015, 1986.

Joanne Y. Law received the B.S. degree in engineering from Brown University, Providence, RI, in 1993 and the M.S.E.E. degree from Stanford University, Stanford, CA, in 1994. She is currently pursuing the Ph.D. degree at the Institute of Optics, University of Rochester, Rochester, NY. Her dissertation work is focused on the dynamic and noise characteristics of vertical-cavity surface-emitting lasers with optical injection and feedback.

Govind P. Agrawal (M'83–SM'86–F'96) received the B.S. degree from the University of Lucknow in 1969 and the M.S. and Ph.D. degrees from the Indian Institute of Technology, New Delhi, in 1971 and 1974, respectively.

After holding positions at the Ecole Polytechnique, France, the City University of New York, New York, and AT&T Bell Laboratories, Murray Hill, NJ, he joined the faculty of the Institute of Optics in 1989 at the University of Rochester, Rochester, NY, where he is a Professor of Optics. His research interests focus on quantum electronics, nonlinear optics, and laser physics. In particular, he has contributed significantly to the fields of semiconductor lasers, nonlinear fiber optics, and optical communications. He is an author or co-author of more than 200 research papers, several book chapters and review articles, and three books, entitled*Semiconductor Lasers* (New York: Van Nostrand Reinhold, 1993), *Nonlinear Fiber Optics* (New York: Academic, 1995), and*Fiber-Optic Communication Systems* (New York: Wiley, 1997). He has also edited the books *Contemporary Nonlinear Optics* (New York: Academic, 1992) and *Semiconductor Lasers: Past, Present and Future* (Woodbury, NY: AIP Press, 1995).

Dr. Agrawal is a Fellow of the Optical Society of America.